Journal of Materials Chemistry A

PAPER

View Article Online
View Journal | View Issue

Cite this: J. Mater. Chem. A, 2018, 6, 24965

Water oxidation catalysed by quantum-sized $BiVO_4$†

Lourdes del Olmo,‡[a] Michael Dommett,‡[b] Ingrid H. Oevreeide,[b] Aron Walsh,[cd] Devis Di Tommaso*[b] and Rachel Crespo-Otero*[b]

Bismuth vanadate $BiVO_4$ is one of the most promising materials for photoelectrochemical water splitting, with recent work highlighting the improved photocatalytic activity of quantum sized $BiVO_4$ compared with the crystalline phase. Herein, we report a theoretical investigation of the structural, optical and catalytic properties of the $(BiVO_4)_4$ clusters through a combination of density functional theory methods (*ab initio* molecular dynamics, time-dependent density functional theory, transition state theory). The enhanced solar water oxidation efficiency of $BiVO_4$ quantum-sized clusters is linked with the localisation of the spin density on the cluster surface, and the dramatic reduction, compared with the crystalline $BiVO_4$ phase, of the Gibbs energy of activation and Gibbs energy of reaction associated with the hydrogen transfer process between water and $BiVO_4$. Our results illustrate the main effects associated with the reduction of dimensions (from bulk to quantum-size) on the main steps of water oxidation mechanisms. This understanding can contribute to the design of efficient $BiVO_4$ quantum sized water-splitting photocatalysts.

Received 17th August 2018
Accepted 26th November 2018

DOI: 10.1039/c8ta08015a

rsc.li/materials-a

Introduction

Hydrogen as a combustible is a clean alternative to traditional energy sources and since the 1970s considerable effort has gone into the development of semiconductor catalysts for the decomposition of water into H_2 and O_2, simultaneously, under simulated solar light irradiation.[1–5]

Bismuth vanadate ($BiVO_4$) represents one of the most promising Z-scheme photocatalysts[6–11] for the hydrogen reduction and water oxidation reactions on separate p-type and n-type electrodes. The monoclinic polymorph displays the highest photocatalytic activity. However, despite possessing the electronic band alignment required to drive solar water oxidation, bulky crystalline $BiVO_4$ shows only modest performance for solar water splitting.[6] This has been associated with poor electron transport, significant electron–hole recombination, and other kinetic factors.

The major kinetic limitation during the photoelectrochemical water splitting is the water oxidation semi-reaction,[12] $2H_2O \rightarrow O_2 + 4H^+ + 4e^-$, which is a multistep, uphill, four-electron, four-proton process:[13]

$$[(BiVO_4) - H_2O] + h\nu \rightarrow [(BiVO_4) - H_2O] + h^+ + e^- \quad (1)$$

$$[(BiVO_4) - H_2O] + h^+ \rightarrow [(BiVO_4) - H_2O]^+ \quad (2)$$

$$[(BiVO_4) - H_2O]^+ \rightleftharpoons [(BiVO_4) - OH] + H^+ (aq) \quad (3)$$

$$[(BiVO_4) - OH] + h^+ \rightleftharpoons [(BiVO_4) - O] + H^+ (aq) \quad (4)$$

$$[(BiVO_4) - O] + H_2O + h^+ \rightleftharpoons [(BiVO_4) - OOH] + H^+ (aq) \quad (5)$$

$$[(BiVO_4) - OOH] + h^+ \rightleftharpoons (BiVO_4) + O_2 + H^+ (aq) \quad (6)$$

The water deprotonation step (3) is generally considered to be rate-determining in water oxidation reactions.[14] Strategies to tune the free energy of activation for this elementary step can help control the solar water oxidation efficiency of $BiVO_4$.

Methods based on metal doping,[15] co-catalyst deposition,[16,17] and semi-conductor recombination[18] have been proposed to enhance the efficiency of crystalline $BiVO_4$ photocatalysts. However, recent work has highlighted the potential of quantum sized $BiVO_4$ photocatalysts for the decomposition of pure water without any co-catalyst or sacrificial reagents.[19] The quantum sized $BiVO_4$ clusters show an improved photocatalytic activity for overall water splitting, which has been associated with quantum confinement effects. Sun and co-workers

[a]Departamento de Química Física Aplicada, Facultad de Ciencias, Universidad Autónoma de Madrid, 28049 Madrid, Spain

[b]Thomas Young Centre and School of Biological Sciences, Queen Mary University of London, Mile End Road, London, E1 4NS, UK. E-mail: d.ditommaso@qmul.ac.uk; r.crespo-otero@qmul.ac.uk

[c]Thomas Young Centre and Department of Materials, Imperial College London, Exhibition Road, London SW7 2AZ, UK

[d]Department of Materials Science and Engineering, Yonsei University, Seoul 03722, Korea

† Electronic supplementary information (ESI) available. See DOI: 10.1039/c8ta08015a

‡ LO and MD contributed equally to this work.

characterised the electronic and optical properties of their synthetic quantum sized $BiVO_4$ using X-ray photoelectron spectroscopy, UV-vis and photoluminescence (PL) spectroscopy. They suggested that the improved photocatalytic activity arises from the negative shift of the conduction band edge. Nevertheless, the fundamental mechanism through which quantum confinement controls the catalytic efficiency of $BiVO_4$ clusters has not been understood fully yet.

Yang *et al.* investigated the mechanism of water oxidation on (010), (110) and (011) facets of $BiVO_4$ using DFT simulations.[20] The authors found a significant facet dependence on the catalytic properties. In recent work, Hu *et al.* also considered the mechanism of water oxidation on the (010) facet of $BiVO_4$ and the role of oxygen vacancies, which facilitated the reaction by decreasing the activation energy barriers of the catalytic reactions.[21]

Since the use of nanoparticle photocatalysts has been proven to be a strong strategy to dramatically improve solar-to-fuel conversion efficiencies,[22–25] understanding the role of size reduction is of fundamental importance in the development of efficient $BiVO_4$ quantum-sized water-splitting photocatalysts. Herein, we report a comprehensive theoretical investigation of the structural and optical properties of a model bismuth vanadate nanoparticle $(BiVO_4)_4$, and a quantification of the initial steps (1–3) in the water-splitting reaction by means of a combination of density functional theory (DFT) methods (*ab initio* molecular dynamics, transition state searching, time-dependent DFT).

Computational details

The initial configuration of $(BiVO_4)_4$ was generated from the most stable termination of the (010) surface of crystalline bismuth vanadate.[9] The cluster was first subjected to 20 ps of *ab initio* (Born-Oppenheimer) molecular dynamics (AIMD) simulations, followed by geometry optimization, both conducted at the PBE level of theory using the DFT plane wave VASP code.[26] This resulted in the reconstruction of the surface and formation of a 3D-closed cage structure expected to be common in nanoparticles (Fig. 1). The structure of this cluster was 190 kJ mol^{-1} more stable than the open structure obtained from direct optimisation at the same level of theory.

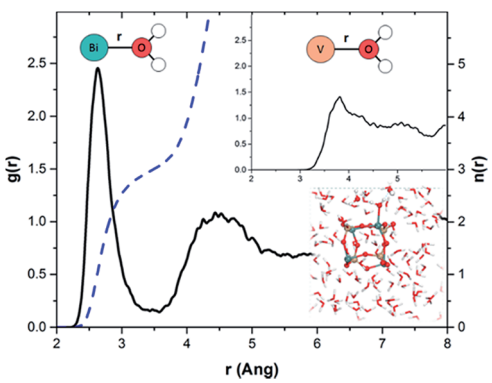

Fig. 1 Bi–O_w radial distribution function (solid line), $g(r)$, and running coordination number (dashed line), $n(r)$, obtained from the AIMD simulations of $(BiVO_4)_4$ in water. Inset: V–O radial distribution function. The hydration of the $(BiVO_4)_4$ cluster in water is also shown, where is highlighted the association of two water molecules to a Bi atom.

AIMD simulations of the hydrated $(BiVO_4)_4$ cluster were conducted with the electronic structure code CP2K/Quickstep, version 2.7.[27,28] CP2K implements DFT based on a hybrid Gaussian plane wave approach. The PBE functional was used with the general dispersion correction termed DFT-D3.[29] Goedecker–Teter–Hutter pseudopotentials were used to describe the core–valence interactions.[30] All atomic species were represented using a double-zeta valence polarised basis set. The plane wave kinetic energy cut off was set to 1000 Ry. The k-sampling was restricted to the Γ point of the Brillouin zone. Simulations were carried out in the canonical (NVT) ensemble at the average temperature of 300 K with a wave function optimization tolerance of 10^{-6} a.u. and a time step of 1 fs. Periodic boundary conditions were applied throughout. The initial configuration was generated starting from a well-equilibrated cubic supercell containing 125 water molecules corresponding to the experimental density of water at room temperature. Fourteen water molecules were then replaced by the optimised structure of $(BiVO_4)_4$ and AIMD simulations were conducted for 5 ps with constrains applied to the initial positions of the cluster. Finally, statistics were collected for a period of 20 ps.

The last snapshot of these AIMD simulations was used to generate hydrated molecular models $(BiVO_4)_4$–$(H_2O)_n$ ($n = 1$–8). These clusters were optimized at B3LYP-D3/def-TZVP level of theory using the Conductor-like Screening Model (COSMO) to simulate the aqueous environment.[31] The excitation step of the water splitting reaction (1) was modelled using time-dependent DFT (TDDFT) with the CAM-B3LYP functional and the def-TZVP basis set. The minimum on the potential energy surface of the first excited state (S_1) was optimised at the same level of theory. The ionisation potentials associated with step (2) were calculated as the energy difference between the cation and neutral clusters. The transition states for the water deprotonated step (3) were located at B3LYP-D3/def-TZVP level. Previous investigations on water splitting mechanisms of Ti and Co clusters have used the same level of theory.[32,33] Harmonic vibrational frequencies were computed for the optimised TS structures to verify the presence of a single imaginary frequency. Intrinsic reaction coordinate calculations were also performed to confirm that the TS structures were connecting reactants and products. Excited state calculations were conducted with the Gaussian09 program[34] whereas TS calculations were carried out with the Turbomole code.[35]

Results

Water coordination

The first step in the water oxidation reaction is the adsorption of H_2O molecules to the photocatalyst. The interaction of water with $(BiVO_4)_4$ was determined from AIMD simulations through the generation of the bismuth–water and vanadium–water radial distribution functions (RDFs), $g(r)$, which represent the probability, relative to a random distribution, of finding an

oxygen water (O_w) at a distance r from the metal atom. The well-defined peak at 2.65 Å in the Bi–O_w RDF and the broad feature in the V–O_w RDF indicate that water molecules interact only with the bismuth atoms of the $(BiVO_4)_4$ cluster (Fig. 1). Integration of the Bi–O_w RDF at the first minimum, 3.5 Å, also reveals that each bismuth atom is coordinated, on average, to three water molecules.

The first minimum of the Bi–O_w RDF does not reach zero indicating that, during the simulation, water molecules move between the first and second coordination shells of the bismuth ions. The application of the "direct" method of Hofer *et al.*[36] to characterize the reactivity of solvated molecules and ions yields a mean residence time of only 1.3 ps for the bismuth ion. The comparison of the average Bi–O_w distance (2.65 Å) with the experimental mean Bi–O_w distance of bismuth(III) ion in aqueous solution (2.41 Å)[37] confirms that in water the $(BiVO_4)_4$ cluster has a very labile hydration structure.

Excitation and ionisation

Microhydrated models were extracted from the final configuration of the AIMD trajectory and optimized with DFT (B3LYP-D3/def-TZVP) in the COSMO solvation model to simulate the aqueous environment. These clusters were used to analyse the excitation and ionisation steps (1 and 2). The hydrated clusters $(BiVO_4)_4$–nH_2O (n = 0–3) were optimized at the TDDFT (CAM-B3LYP/def-TZVP) level of theory in the first excited state (S_1). The formation of the cation from the neutral cluster, step (2), was characterized in terms of the ionisation potentials (IP^{BiVO_4}) of the bare and hydrated clusters, $(BiVO_4)_4$–nH_2O (n = 1–8) (Fig. 2). The optimized structures of clusters are displayed in the ESI.†

The vertical ionisation potential of the bare $(BiVO_4)_4$ cluster is 9.3 eV. Geometry relaxation of the cation decreases the ionisation potential to 8.7 eV. We have previously shown that water adsorption can tune the position of the edge bands.[38,39] Fig. 2 illustrates the effect of increasing the number of water molecules on the ionisation potentials the $(BiVO_4)_4$.

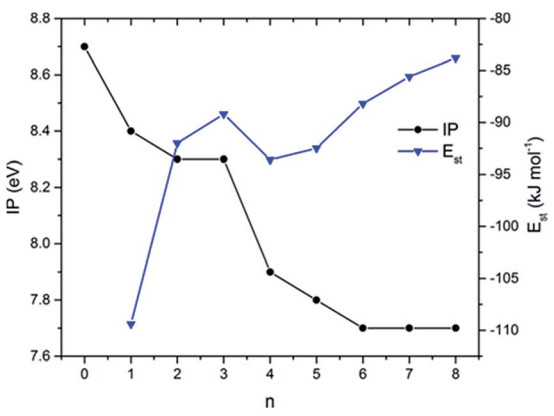

Fig. 2 Ionisation potentials calculated considering the relaxation of the clusters in their cationic forms. Stabilization energies/per water molecule for clusters of n = 1–8 by the number of water molecules and ionisation potentials.

The interaction between water and $(BiVO_4)_4$ decreases the ionisation potential from 8.7 eV for the bare cluster to 7.7 eV for $(BiVO_4)_4$–$8H_2O$ (Fig. 2). This decrease of the ionisation potential is likely to be related with the electrostatic interactions of $(BiVO_4)_4$ with the water molecules. As shown in Fig. 2, the stabilisation energy of the clusters per water molecule increases with the number of water molecules. The ionisation potential for the (010) surface of $BiVO_4$ is 7.3 eV, according to recent photoemission experiments[40] and simulations.[9,41]

To analyse the position of the hole after ionisation, we considered the spin density of the cationic species. As shown in Fig. 3 for $[(BiVO_4)_4$–$8H_2O]^+$, ionisation involves localisation of the spin density, in particular on the terminal oxygen, with the linking oxygen playing minor roles. No overall effect from the water molecules on the spin densities is observed, regardless the number of water molecules, and can be associated with the localisation of the electronic density on the cluster surface (see Fig. 4 for $[(BiVO_4)_4$–$3H_2O]^+$). This is essential to explain the larger reactivity of the cluster with respect to the solid surface.

Fig. 4 illustrates different steps in the mechanism for the $[(BiVO_4)_4$–$3H_2O]$ cluster, which was suggested as one of the most common configurations in our dynamics simulations. The electron–hole separation induced by light step (1) involves the oxygen and vanadium atoms of one of the VO_4 groups (Fig. 4). The electron density is localised on one extreme of the cluster and, similarly to the ionisation, is not significantly affected by the water molecules.

In step (2) ionisation removes the electron from the two oxygens initially excited (see spin densities in Fig. 3 and 4). This picture agrees with the features of both the bulk material and the (010) surface, where the main contribution to the valence band is from the oxygen 2p orbitals, while V conduction is dominated by V 3d orbitals.[38] A significant degree of localisation of the hole is found for the quantum cluster in contrast with the delocalisation found for the bulk and surface. A recent investigation of bigger clusters of $BiVO_4$ also found that the HOMO and LUMO densities where significantly localised on a few atoms on the cluster surface.[42]

We consider the effect of hydroxyl adsorption by calculating the ionisation potentials of the clusters: $[(BiVO_4)_4$–$OH]^-$ and $[(BiVO_4)_4$–$OH(H_2O)]^-$. These calculations show that hydroxyl

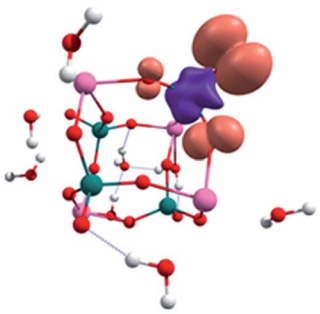

Fig. 3 Spin density map for the $[(BiVO_4)_4$–$8H_2O]^+$ cation obtained at CAM-B3LYP/def-TZVP level of theory. Positive: orange, negative: magenta.

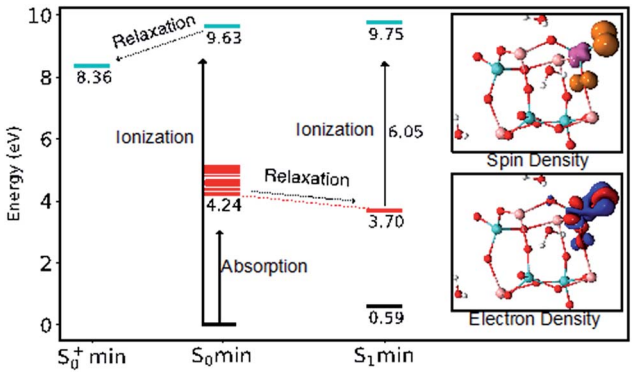

Fig. 4 Excited state mechanism for $(BiVO_4)_4$–$3H_2O$ cluster. Inset; electron density difference map (S_0: blue, S_1: red) at the S_1 minimum, and post ionisation spin density map (positive: orange, negative: magenta). Energies and geometries were obtained at (TD-)CAM-B3LYP/def-TZVP level of theory.

adsorption significantly changes the energy levels of the clusters; the obtained ionisation potentials are 6.13 eV for $[(BiVO_4)_4$–$OH]^-$ and 5.66 eV for $[(BiVO_4)_4$–$OH(H_2O)]^-$ respectively. Given that the excitation energies obtained for these clusters (4.01 and 4.11 eV) are similar to those for the hydrated ones, the reason for the smaller ionisation potentials is likely to be associated with the destabilisation of the valence band because of OH adsorption. In contrast with the neutral molecule, a more important fraction of the hole is on the water molecule (Fig. S3, ESI†). However, we should highlight that the molecular dynamics AIMD simulations show that consequently for neutral conditions the water molecules adsorbed on the bismuth vanadate cluster do not spontaneously dissociate and, consequently, at neutral conditions the will not be a significant amount of hydroxyls adsorbed at the surface is unlikely to be significant.

The optical properties of $BiVO_4$ particles strongly depend on the sample preparation and particles size. The experimental band gap of $BiVO_4$ nanoclusters is in the range of 3.51–3.67 eV or 2.75–2.82 eV.[43,44] The quantum sized $BiVO_4$ particles synthesised by Sun *et al.* show a broad adsorption band in the visible region with the maximum of adsorption (300 m, 4.1 eV) in the near UV region. The position of the inflexion points is significantly shifted with respect to the value from the nanoscale particles (from 465 nm to 365 nm). Their quantum sized particles have a band gap of 2.72 eV while the value for bigger nanoparticles is 2.4 eV.[45] Because of quantum confinement, the optical gaps of both anhydrous and hydrated $(BiVO_4)_4$ cluster are wider than the values for bulk and the (010) surface of monoclinic bulk.[9,46,47]

From the ground state equilibrium geometry, excitation to the first twenty-five excited states ranges between 4–5 eV. The optical gap of the $(BiVO_4)_4$–$3H_2O$ cluster is 4.24 eV (Fig. 4) (n = 0: 4.32, n = 1: 4.25, n = 2: 4.25), which is wider than the band gap but close to the maximum of adsorption of the quantum particles.[45] The optical gap reduces to 3.1 eV (400 nm) after relaxation in S_1. This can be compared with the photoluminescence spectrum of the quantum-sized particles that expands from 470 to 600 nm with six emission peaks centred around 382, 399, 425, 450 and 491 nm. These peaks have been associated with the discontinuous emission from discrete levels. The optical properties of the quantum sized micro-hydrated $BiVO_4$ system considered in our theoretical work are therefore representative of the PL spectra measured by Sun and co-workers.[45]

Fig. 4 summarises the steps for the electrochemical process for the $[(BiVO_4)_4$–$3H_2O]$ cluster. Vertical ionisation from the ground state minimum occurs at 9.63 eV. After relaxation in the cationic state, the ionisation potential reduces to 8.63 eV (as shown before these values are smaller when more water molecules are included, we are only interested here in the general qualitative description). This promotes and electron–hole separation within one of the VO_4 subunits.

Alternatively, if we consider the photo-electrochemical process, after excitation the cluster can relax in the excited state from where the energy required for ionisation is smaller (6.05 eV). Our calculations show a significant localisation of the hole on the surface of the cluster. This is one of the most significant effects of reducing the size from bulk to nanoscale to quantum size. The next step is the catalytic reaction with the cation, which we analyse in the next section.

Catalysis

Since no proton transfer was observed between water and $(BiVO_4)_4$ during the AIMD simulations (Fig. 1), the deprotonation step (3) should be an activated process. We consider the transition states associated with the deprotonation step (3) of the clusters with one and two water molecules: $[(BiVO_4)_4$–$H_2O]$ and $[(BiVO_4)_4$–$2H_2O]$ in their neutral and cationic forms. One question to answer is whether the second water molecule has a catalytic role or acts as a reactant in the water oxidation mechanism.

We investigate two possible reaction pathways: A, where the hydrogen (H) transfer occurs between the water molecule and the oxygen atom bound to vanadium; B, where the proton is transferred to the bridging Bi–O–V oxygen (Fig. 5). As expected

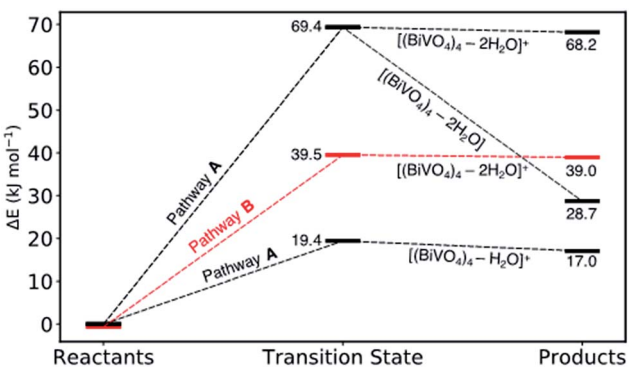

Fig. 5 Energy profiles for deprotonation of water *via* pathways A and B for the neutral and cationic $BiVO_4$ clusters, with one or two explicit water molecules, as computed at the B3LYP-D3/def-TZVP level of theory in water using the COSMO solvation model.

all mechanisms are uphill consequently either electrochemical potential or light is needed for the reactions to proceed.

Fig. 6 shows the structure of the reactants, transition states and products for the two lowest energy pathways. In the case of the neutral model, we could only locate one transition state associated with pathway A, requiring 69.4 kJ $mol^{-1}$to proceed, producing a high energy product (Fig. 5), which is similar to the energy obtained for $[(BiVO_4)_4–2H_2O]^+$ for pathway A. In contrast, the only transition state associated with pathway B was found for the $[(BiVO_4)_4–2H_2O]^+$ cluster with an activation barrier of 39.5 kJ mol^{-1} ($\Delta G^* = 10.8$ kJ mol^{-1}). This is because the structure of the hydrogen bonding between the two water molecules helps stabilise the cyclic transition state.

Overall, the reaction through pathway A for $[(BiVO_4)_4–H_2O]^+$ is more favourable kinetically and thermodynamically. The barrier of the reaction is 19.4 kJ mol^{-1} ($\Delta G^* = 7.4$ kJ mol^{-1}). The product of the reaction involves the stabilisation of the Bi–OH bond and the weakening of a vicinal Bi–O bridge bond (from 2.48 to 2.60 Å). The relatively small barrier for this reaction with respect to the pathway B for $[(BiVO_4)_4–2H_2O]^+$ can be explained considering that the larger contribution to the hole is on the surface O, while the bridging O has a smaller contribution.

The energies of the intermediates for deprotonation reaction catalysed by crystalline $BiVO_4$ obtained by Yang *et al.*[14] are 115 and 270 kJ mol^{-1} (2.37 and 2.25 eV) for (010) and (011) facets respectively and the free energies considering the reference to the NHE are 46.3 kJ mol^{-1} and 29.0 kJ mol^{-1}.[14] In these studies, no transition state was found and only the thermodynamics of the reaction was considered. These reactions have a late transition state (Fig. 5), and therefore the energy of the intermediates provides the lowest limit of their transition state energies.

Our calculations show that the quantum-sized $(BiVO_4)_4$ cluster has the ability to drastically reduce the endoergonicity of the water deprotonation reaction compared with the bulky crystalline $BiVO_4$. The reason for the larger reactivity of the clusters seems to be the localisation of the hole on the surface of the cluster facilitating the deprotonation reaction. However, this localisation comes at the expense of an increase in the band gap and adsorption energies that have to be controlled for an overall positive outcome of the reaction. The control of these interconnected factors is required for the design of more efficient materials for water oxidation.

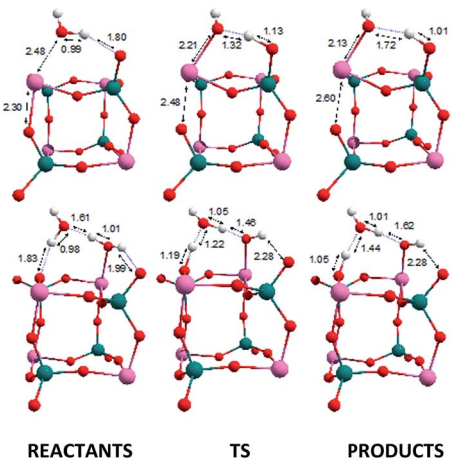

Fig. 6 From left to right: optimised structures of the reactant, transition state and product along pathway A $[(BiVO_4)–H_2O]^+$(top) and pathway B $[(BiVO_4)–2H_2O]^+$ (bottom). Calculations conducted using the B3LYP-D3/def-TZVP/COSMO method.

Conclusions

Investigation of the structural, optical, and catalytic properties of the $(BiVO_4)_4$ nanoparticle in water has been conducted by means of computer simulations based on density functional theory. *Ab initio* molecular dynamics simulations of hydrated $(BiVO_4)_4$ show that water molecules adsorb only to the bismuth atoms with the $(BiVO_4)_4$ cluster being characterized by a very labile hydration structure.

Time dependent DFT calculations of microhydrated $(BiVO_4)_4–nH_2O$ (n = 1–8) models extracted from the AIMD trajectory were used to model the excitation (1) and ionisation (2) steps of the water oxidation semi-reaction. These calculations show that ionisation involves localisation of the spin density on the cluster surface, particularly on the terminal oxygen with the linking oxygen playing minor roles, explaining the larger reactivity of the cluster with respect to the solid surface.

Finally, static DFT localisation of the reactant, transition state and products on the potential energy surface of the water deprotonation step (3). There is a dramatic reduction, compared with the crystalline $BiVO_4$ phase, of the activation energy of reaction associated with the hydrogen transfer process between water and $(BiVO_4)_4$ cluster. In conclusion, this computational study demonstrates the root of the improved performance of $BiVO_4$ quantum sized clusters compared with the crystalline phase.

Conflicts of interest

There are no conflicts to declare.

Acknowledgements

We are grateful to the UK Materials and Molecular Modelling Hub for computational resources, which is partially funded by EPSRC (EP/P020194/1). IHO and RCO acknowledge Royal Society of Chemistry for an Undergraduate Research Bursary (2015). We would like to thank Jose Manuel Garcia de la Vega for his support. This research utilized Queen Mary's Apocrita HPC facility, supported by QMUL Research-IT.

References

1 A. Fujishima and K. Honda, *Nature*, 1972, **213**, 8656.
2 K. Maeda, *ACS Catal.*, 2014, **4**, 1632–1636.
3 *Photoelectrochemical Water Splitting*, ed. H.-J. Lewerenz and L. Peter, The Royal Society of Chemistry, 2014.
4 L. M. Peter and K. G. Upul Wijayantha, *ChemPhysChem*, 2014, **15**, 1983–1995.

5 M. M. May, H.-J. Lewerenz, D. Lackner, F. Dimroth and T. Hannappel, *Nat. Commun.*, 2015, **6**, 8286.
6 T. W. Kim and K.-S. Choi, *Scienc*, 2014, **343**, 990–994.
7 Y. Park, K. J. McDonald and K.-S. Choi, *Chem. Soc. Rev.*, 2013, **42**, 2321–2337.
8 S. M. Thalluri, C. Martinez Suarez, S. Hernández, S. Bensaid, G. Saracco and N. Russo, *Chem. Eng. J.*, 2014, **245**, 124–132.
9 R. Crespo-Otero and A. Walsh, *J. Phys. Chem. Lett.*, 2015, **6**, 2379–2383.
10 K. E. Kweon, G. S. Hwang, J. Kim, S. Kim and S. Kim, *Phys. Chem. Chem. Phys.*, 2014, **17**, 256–260.
11 H. L. Tan, X. Wen, R. Amal and Y. H. Ng, *J. Phys. Chem. Lett.*, 2016, **7**, 1400–1405.
12 D. K. Zhong, S. Choi and D. R. Gamelin, *J. Am. Chem. Soc.*, 2011, **133**, 18370–18377.
13 H. Inoue, T. Shimada, Y. Kou, Y. Nabetani, D. Masui, S. Takagi and H. Tachibana, *ChemSusChem*, 2011, **4**, 173–179.
14 J. Yang, D. Wang, X. Zhou and C. Li, *Chemistry*, 2013, **19**, 1320–1326.
15 H. S. Park, K. E. Kweon, H. Ye, E. Paek, G. S. Hwang and A. J. Bard, *J. Phys. Chem. C*, 2011, **115**, 17870–17879.
16 J. H. Kim, J. W. Jang, H. J. Kang, G. Magesh, J. Y. Kim, J. H. Kim, J. Lee and J. S. Lee, *J. Catal.*, 2014, **317**, 126–134.
17 K. R. Yoon, J. W. Ko, D.-Y. Youn, C. B. Park and I.-D. Kim, *Green Chem.*, 2016, **18**, 944–950.
18 I. Grigioni, K. G. Stamplecoskie, E. Selli and P. V Kamat, *J. Phys. Chem. C*, 2015, **119**, 20792–20800.
19 S. Sun, W. Wang, D. Li, L. Zhang and D. Jiang, *ACS Catal.*, 2014, **4**, 3498–3503.
20 J. Yang, D. Wang, X. Zhou and C. Li, *Chem.–A Eur. J.*, 2013, **19**, 1320–1326.
21 J. Hu, X. Zhao, W. Chen, H. Su and Z. Chen, *J. Phys. Chem. C*, 2017, **121**, 18702–18709.
22 Z. Li, J. Feng, S. Yan and Z. Zou, *Nano Today*, 2015, **10**, 468–486.
23 R. V Gonçalves, H. Wender, S. Khan and M. A. Melo, *Nanoenergy: Nanotechnology Applied for Energy Production*, ed. F. L. Souza and E. R. Leite, Springer International Publishing, Cham, 2018, pp. 107–140.
24 B. Liu and X. Zhao, *Phys. Chem. Chem. Phys.*, 2014, **16**, 22343–22351.
25 M. Ogawa and H. Kaiho, *Langmuir*, 2002, **18**, 4240–4242.
26 G. Kresse and J. Furthmüller, *Comput. Mater. Sci.*, 1996, **6**, 15–50.
27 J. Hutter, M. Iannuzzi, F. Schiffmann and J. VandeVondele, *Wiley Interdiscip. Rev.: Comput. Mol. Sci.*, 2014, **4**, 15–25.
28 D. Frenkel and B. Smit, *Understanding Molecular Simulation: From Algorithms to Applications, Comp. Sci. series*, Academic Press, 2001.
29 S. Grimme, J. Antony, S. Ehrlich and H. Krieg, *J. Chem. Phys.*, 2010, **132**, 154104.
30 S. Goedecker, M. Teter and J. Hutter, *Phys. Rev. B*, 1996, **54**, 1703–1710.
31 K. Andreas, *Wiley Interdiscip. Rev.: Comput. Mol. Sci.*, 2017, **8**, e1338.
32 A. Kazaryan, R. van Santen and E. J. E. J. Baerends, *Phys. Chem. Chem. Phys.*, 2015, **17**, 20308–20321.
33 M. Schilling, G. R. Patzke, J. Hutter and S. Luber, *J. Phys. Chem. C*, 2016, **120**, 7966–7975.
34 M. J. Frisch, G. W. Trucks, H. B. Schlegel, G. E. Scuseria, M. A. Robb, J. R. Cheeseman, G. Scalmani, V. Barone, G. A. Petersson, H. Nakatsuji, X. Li, M. Caricato, A. Marenich, J. Bloino, B. G. Janesko, R. Gomperts, B. Mennucci, H. P. Hratchian, J. V. Ortiz, A. F. Izmaylov, J. L. Sonnenberg, D. Williams-Young, F. Ding, F. Lipparini, F. Egidi, J. Goings, B. Peng, A. Petrone, T. Henderson, D. Ranasinghe, V. G. Zakrzewski, J. Gao, N. Rega, G. Zheng, W. Liang, M. Hada, M. Ehara, K. Toyota, R. Fukuda, J. Hasegawa, M. Ishida, T. Nakajima, Y. Honda, O. Kitao, H. Nakai, T. Vreven, K. Throssell, J. A. Montgomery Jr, J. E. Peralta, F. Ogliaro, M. Bearpark, J. J. Heyd, E. Brothers, K. N. Kudin, V. N. Staroverov, T. Keith, R. Kobayashi, J. Normand, K. Raghavachari, A. Rendell, J. C. Burant, S. S. Iyengar, J. Tomasi, M. Cossi, J. M. Millam, M. Klene, C. Adamo, R. Cammi, J. W. Ochterski, R. L. Martin, K. Morokuma, O. Farkas, J. B. Foresman and D. J. Fox, *Gaussian 09*, Gaussian Inc., Wallingford CT, 2016.
35 R. Ahlrichs, M. Bär, M. Häser, H. Horn and C. Kölmel, *Chem. Phys. Lett.*, 1989, **162**, 165–169.
36 T. S. Hofer, H. T. Tran, C. F. Schwenk and B. M. Rode, *J. Comput. Chem.*, 2004, **25**, 211–217.
37 J. Näslund, I. Persson and M. Sandström, *Inorg. Chem.*, 2000, **39**, 4012–4021.
38 R. Crespo-Otero and A. Walsh, *J. Phys. Chem. Lett.*, 2015, **6**, 2379–2383.
39 K. T. Butler, R. Crespo-Otero, J. Buckeridge, D. O. Scanlon, E. Bovill, D. Lidzey and A. Walsh, *Appl. Phys. Lett.*, 2015, **107**, 231605.
40 J. K. Cooper, S. Gul, F. M. Toma, L. Chen, P.-A. Glans, J. Guo, J. W. Ager, J. Yano and I. D. Sharp, *Chem. Mater.*, 2014, **26**, 5365–5373.
41 F. Ambrosio, J. Wiktor and A. Pasquarello, *ACS Energy Lett.*, 2018, **3**, 829–834.
42 K. Ordon, A. Kassiba and M. Makowska-Janusik, *RSC Adv.*, 2016, **6**, 110695–110705.
43 S. Sarkar and K. K. Chattopadhyay, *Phys. E*, 2012, **44**, 1742–1746.
44 S. Sarkar, N. S. Das and K. K. Chattopadhyay, *Solid State Sci.*, 2014, **33**, 58–66.
45 S. Sun, W. Wang, D. Li, L. Zhang and D. Jiang, *ACS Catal.*, 2014, **4**, 3498–3503.
46 Z. Zhao, Z. Li and Z. Zou, *Phys. Chem. Chem. Phys.*, 2011, **13**, 4746–4753.
47 K. Ding, B. Chen, Y. Li, Y. Zhang and Z. Chen, *J. Mater. Chem. A*, 2014, **2**, 8294.

